Effect of Sc and Zr Additions on Dispersoid Microstructure and Mechanical Properties of Hot-Rolled AA5083

Ahmed Y. Algendy, Kun Liu, Paul Rometsch, Nick Parson, and X.-Grant Chen

Abstract

5xxx aluminum alloys are traditionally considered non-heat-treatable. With the addition of Sc/Zr and multistep heat treatment, two kinds of dispersoids (AlMn and $Al_3(Sc,Zr)$) were formed. The effect of Sc additions (0.08–0.43 wt.%) on dispersoid formation and mechanical properties of hot-rolled sheets was investigated. The results showed that tensile properties initially increased with increasing Sc addition. The yield strength (YS) and ultimate tensile strength (UTS) of the alloy with 0.16 wt.% Sc reached 295 and 411 MPa, respectively, showing improvements of 28% in YS and 8% in UTS compared to the base alloy. However, with a further increase of Sc, the tensile properties declined owing to the formation of a line/fan-shaped microstructure associated with discontinuous $Al_3(Sc,Zr)$ precipitation during solidification. The evolution of $Al_3(Sc,Zr)$ and AlMn dispersoids during heat treatment and hot rolling was characterized using scanning and transmission electron microscopies. Their influence on the mechanical properties of hot-rolled AA5083 alloys was discussed.

Keywords

Aluminum 5083 alloy • Sc and Zr addition • Dispersoids • Mechanical properties

Introduction

Owing to their excellent combination of high strength-to-weight ratio, good formability, high toughness, excellent weldability and corrosion resistance, Al-Mg-Mn 5xxx alloys are considered excellent candidates for transportation and construction industries [1, 2]. Traditionally, 5xxx aluminum alloys are classified as non-heat-treatable alloys. Therefore, the achievable strength of this alloy series is more limited than that of heat-treatable high-strength aluminum alloys. Microalloying with Sc can significantly improve the mechanical properties, preserve the work hardening and enhance the recrystallization resistance of Al-Mg-Mn 5xxx alloys [3, 4]. Owing to its cost-effectiveness, Zr is often added together with Sc. The combination of Sc and Zr can form core–shell $Al_3(Sc_{1-x},Zr_x)$ precipitates with the same $L1_2$-crystal structure of Al_3Sc while improving coarsening resistance [5].

In addition to work hardening and solid solution strengthening, dispersoid strengthening can provide a significant potential for improving the mechanical strength of non-heat-treatable aluminum alloys, such as 3xxx [6, 7] and 5xxx [8] alloys. Recent studies in AA3004 and AA5083 alloys demonstrated that a multistep heat treatment can be used to promote the precipitation of submicron-sized Mn-bearing dispersoids and nano-sized $Al_3(Sc,Zr)$ dispersoids, resulting in enhanced mechanical properties [8–10]. In Al-Mg-Mn 5xxx alloys, the precipitation temperatures of AlMn dispersoids and $Al_3(Sc,Zr)$ precipitates are similar, and both phases are coarsening-resistant, which provides a common basis for improving the mechanical properties during heat treatment. However, there is little information on the synergetic effects of these strengthening phases in 5xxx alloys.

With additions of Sc and Sc + Zr, $Al_3Sc/Al_3(Sc,Zr)$ precipitates can be formed either continuously or discontinuously [11, 12]. Continuous precipitation usually occurs during aging (300–400 °C), in which nano-sized $Al_3Sc/$

A. Y. Algendy · K. Liu · X.-G. Chen (✉)
Department of Applied Science, University of Quebec at Chicoutimi, Saguenay, QC G7H 2B1, Canada
e-mail: xgrant_chen@uqac.ca

P. Rometsch · N. Parson
Arvida Research and Development Center, Rio Tinto Aluminium, Saguenay, QC G7S 4K8, Canada

S. Broek (ed.), *Light Metals 2023*, The Minerals, Metals & Materials Series,
https://doi.org/10.1007/978-3-031-22532-1_165

Al_3(Sc,Zr) precipitates effectively retard the dislocation and grain boundary movements and significantly improve the alloy properties [5, 13]. However, discontinuous precipitation can also occur during solidification with rod- and lamellae-like morphologies [14, 15]. The tendency of Al-Sc/Zr alloys to form Al_3Sc/Al_3(Sc,Zr) discontinuous precipitates is strongly related to their Sc level (often in high-Sc hypereutectic alloys) [12, 15] and solidification rate [14, 16]. Most studies considered Al_3Sc/Al_3(Sc,Zr) discontinuous precipitates as an undesirable microstructure feature, which negatively affects the mechanical properties of the alloy.

This study investigated the effect of Sc additions (0.08–0.43 wt.%) on the precipitation behavior of dispersoids and mechanical properties in a typical Al-Mg-Mn AA5083 alloy during thermomechanical processing (heat treatment and hot rolling). To clarify the roles of micro-alloyed Sc and Zr, the microstructural evolution after heat treatment and hot rolling was characterized by scanning electron microscopy (SEM) and transmission electron microscopy (TEM).

Methodology

Four Al-Mg-Mn alloys were prepared according to the typical AA5083 chemical composition with various Sc and Zr levels, denoted as the Base, Sc08, Sc15, and Sc43 following their Sc levels. The chemical compositions of the experimental alloys, as analyzed by optical emission spectroscopy, are shown in Table 1. The alloys were prepared in an electrical resistance furnace, and the melt was cast in a permanent steel mold preheated at 250 °C with a cooling rate of 2 °C/s to produce cast ingots with a dimension of 30 × 40 × 80 mm.

After casting, all alloys were subjected to a three-step heat treatment (275 °C/12 h + 375 °C/48 h + 425 °C/12 h) to promote the precipitation of AlMn-dispersoids and Al_3(Sc, Zr) precipitates and to improve the processability of rolling [8, 10]. After heat treatment, the samples were hot-rolled at 500 ± 20 °C to a final thickness of 3.2 mm (87% reduction) using a laboratory-scale rolling mill. After rolling and before mechanical testing, all rolled sheets were annealed at 300 °C for 5 h to relieve the rolling-induced thermal stress.

The Vickers microhardness was measured at room temperature with a load of 10 g and a 20 s dwell time. The average value was calculated from 20 measurements for each sample. Uniaxial tensile tests were conducted using an Instron 8801 servo-hydraulic testing unit at a strain rate of 0.5 mm/min. The tensile samples were machined according to ASTM E8/ E8M-16a in the rolling direction with a gauge length of 32 mm and gauge area of 3 × 6 mm. Average results were obtained from three repeated tests.

The microstructure evolution was characterized using scanning electron microscopy (SEM, JSM-6480LV) and transmission electron microscopy (TEM, JEM-2100). In addition, the cast samples were etched with Keller's reagent for 30 s to highlight the discontinuous precipitates. Image analysis with ImageJ software was used for measuring the area fraction of intermetallic particles, the size and number density of the AlMn dispersoids and Al_3(Sc,Zr) precipitates. The number density was measured according to Eq. 1 [8, 10]

$$ND = \frac{N}{A * (D + t)} \quad (1)$$

where; N is the number of particles in the TEM image, A is the total area, D is the equivalent diameter, and t is the thickness of the TEM foil. Finally, the grain structure was mapped and analyzed after rolling and annealing using the Electron Back-Scatter Diffraction (EBSD) technique with a step size of 1 μm.

Results and Discussion

Evolution of the Microstructure in the As-Cast and Heat Treatment

Figure 1 displays the as-cast microstructure of the experimental alloys after Keller etching. The microstructure is mainly composed of the α-Al matrix surrounded by intermetallic phases distributed along the interdendritic regions. The three major intermetallic compounds (IMC) in the experimental alloys were Fe/Mn-rich phases (α-Al_{15}(Fe, Mn)$_3Si_2$ and Al_6(Fe,Mn)), and primary Mg_2Si as identified by SEM-EDS. A small amount of the low melting point eutectic phases, τ-Al_6CuMg_4 and β-Al_5Mg_3, was also

Table 1 Chemical composition of experimental alloys

Alloys	Elements, wt.%								
	Mg	Mn	Si	Fe	Cu	Cr	Ti	Sc	Zr
Base	4.78	0.79	0.26	0.31	0.12	0.14	0.09	–	–
Sc08	4.76	0.79	0.26	0.35	0.10	0.15	0.10	**0.08**	**0.08**
Sc15	4.75	0.81	0.31	0.31	0.11	0.15	0.09	**0.16**	**0.17**
Sc43	4.76	0.75	0.30	0.33	0.10	0.15	0.10	**0.43**	**0.15**

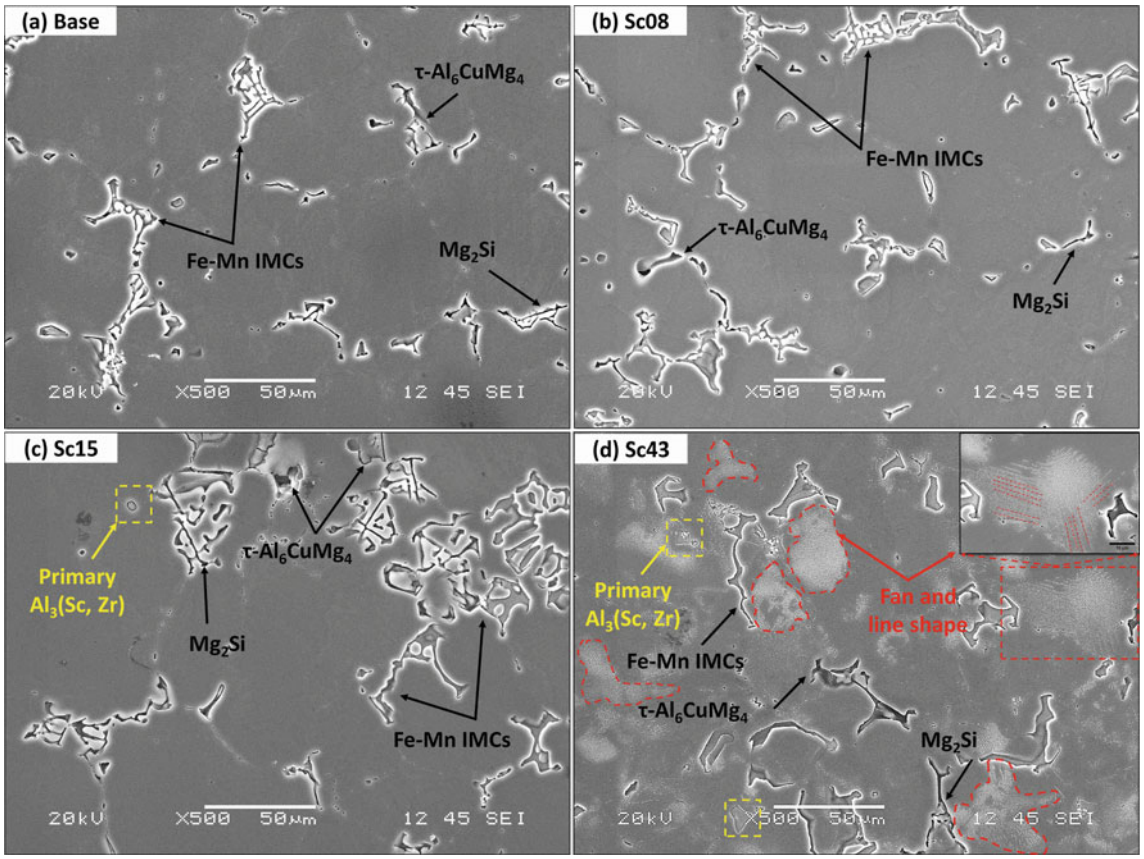

Fig. 1 SEM images showing the as-cast microstructure evolution with Sc and Zr content after etching with Keller's reagent

detected along the interdendritic regions. Furthermore, the area fraction of Fe/Mn-rich intermetallic and Mg_2Si remarkably increased with the Sc and Zr addition. For instance, the area fractions of Fe/Mn-rich and Mg_2Si IMCs increased from 1.98%, 0.7% in the base alloy to 2.31%, 0.77% in alloy Sc08, and further to 3.14%, 0.9% in alloy Sc15. This could be attributed to the reduction of Mn and Mg solubility associated with the addition of Sc and Zr [17, 18].

In addition, in the Sc-containing alloys (Sc15 and Sc43), a few primary $Al_3(Sc,Zr)$ particles were detected inside the aluminum dendrite cells and their fraction increased with increasing Sc content (Fig. 1 c and d). Furthermore, in the alloy Sc43 with the highest Sc content (0.43%), several areas exhibited the formation of fan- and line-shaped aggregates (marked by red dashed lines in Fig. 1d), which was rarely observed in the Sc08/Sc15 alloy. This type of precipitate was related to the decomposition of the supersaturated solid solution to form discontinuous $Al_3(Sc,Zr)$ precipitates (DCP) at a moving grain boundary. More details on the discontinuous precipitation mechanism were reported in our previous study [19].

After heat treatment, the low-melting-point eutectic phases (τ-Al_6CuMg_4/β-Al_5Mg_3) were entirely dissolved in the aluminum matrix with a partial dissolution of Mg_2Si in all cases. Meanwhile, a large number of duplex precipitation populations (AlMn dispersoids and $Al_3(Sc,Zr)$ precipitates) were formed, as shown in Fig. 2. Bright-field TEM images in Fig. 2 a-d show the precipitation of submicron-sized Mn-dispersoids; their size and number density are quantified in Table 2. The types of AlMn dispersoids were identified as Al_4Mn and Al_6Mn based on SADP and TEM-EDS analysis in our previous work [8]. With increasing Sc and Zr contents, the size of the dispersoids increased, and the number density decreased. For instance, the equivalent diameter of AlMn dispersoids in the base alloy was $\sim$25 nm and the number density was $\sim 56 \times 10^{20}$ m^{-3}, while the diameter of dispersoids in the Sc15 alloy increased to $\sim$33.5 nm and the number density decreased to 30×10^{20} m^{-3} (Table 2). There are two possible reasons for increasing the size and decreasing the number density of AlMn dispersoids in Sc-containing alloys. First, adding Sc and Zr reduces the solubility of Mn, Mg, and Si in the aluminum matrix [17, 18]. Secondly, the addition decreases the nucleation efficiency of AlMn dispersoids during heat treatment by decreasing the nucleation sites in the first stage (275 °C/12 h) [20, 21].

In addition to the AlMn-dispersoids, a large number of nano-sized, spherical $Al_3(Sc,Zr)$ precipitates were also

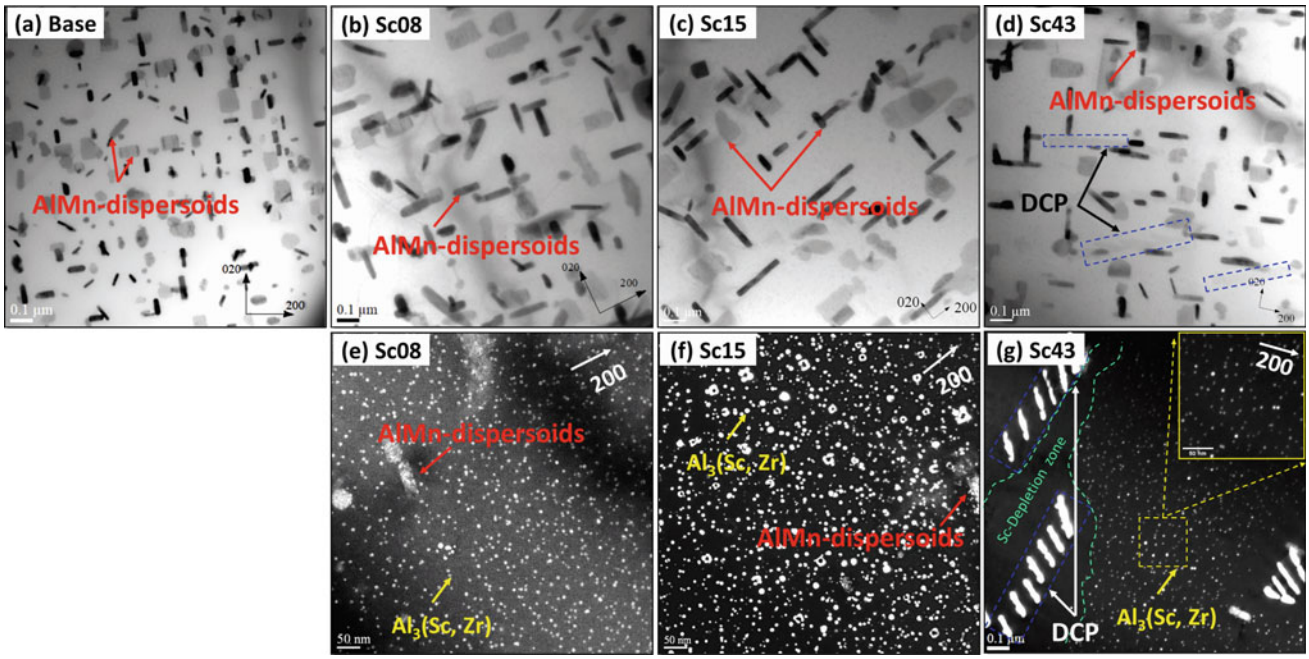

Fig. 2 Bright-field TEM images (**a**, **b**, **c**, **d**) showing the distribution of AlMn dispersoids for Base, Sc08, Sc15 and Sc43; dark-field TEM images (**e**, **f**, **g**) showing the distribution of $Al_3(Sc,Zr)$ precipitates for Sc08, Sc15 and Sc43

Table 2 Quantitative measurements of AlMn dispersoids and $Al_3(Sc,Zr)$ after heat treatment and rolling

Alloy	After heat treatment				After rolling and annealing			
	AlMn dispersoids		$Al_3(Sc,Zr)$		AlMn dispersoids		$Al_3(Sc,Zr)$	
	d (nm)	N_d (10^{20}/m^3)	d (nm)	N_d (10^{22}/m^3)	d (nm)	N_d (10^{20}/m^3)	d (nm)	N_d (10^{22}/m^3)
Base	24.8 ± 1.7	55.9 ± 22.2	–	–	32.4 ± 0.2	23.1 ± 46	–	–
Sc08	29.6 ± 5	30.9 ± 64.0	5.3 ± 0.5	11.3 ± 683	57.2 ± 0.6	6.01 ± 9.6	11.9 ± 0.5	2.7 ± 385
Sc15	33.5 ± 2.6	30.1 ± 56.7	6.1 ± 1.2	19.7 ± 741	56.0 ± 0.6	6.48 ± 13.3	12.6 ± 0.4	5.7 ± 297
Sc43	33.6 ± 1.6	28.7 ± 21.2	8.3 ± 1.4	5.2 ± 741	64.6 ± 1.7	6.80 ± 11.3	37.8 ± 2.6	0.7 ± 177

formed in the Sc-containing alloys, as shown in the dark-field TEM images in Fig. 2e–g. The $Al_3(Sc,Zr)$ precipitates were much finer with a higher number density than the AlMn-dispersoids, and were uniformly distributed in the Al matrix. These precipitates filled the space between the AlMn dispersoids, lowering the inter-particle distance, and resulting in more obstacles for dislocation movements. In addition, Fig. 2d, g revealed a number of rod-like precipitates, non-uniformly distributed in the Al matrix, which originally came from the as-cast fan- and line-shaped microstructure (Fig. 1d) but were partially dissolved during the heat treatment. Those rod-like precipitates were discontinuous precipitates of $Al_3(Sc,Zr)$ (DCP) formed during solidification [15, 19], and their size was much larger than the spherical ones. Furthermore, as shown in Fig. 2g (marked by green dashed lines), there were almost no spherical $Al_3(Sc,Zr)$ precipitates in the vicinity of the rod-like discontinuous precipitates.

The image analysis results in Table 2 show that the number density of spherical $Al_3(Sc,Zr)$ precipitates initially increased with increasing Sc content to 0.16 wt.% (Sc15) and then decreased with increasing Sc to 0.43 wt.% (Sc43). The reason for this effect is that the formation of discontinuous precipitates consumed large amounts of Sc and Zr solutes, decreasing the Sc and Zr content in the solid solution. Furthermore, it created a depleted zone surrounding the rod-like precipitates, preventing further precipitation of the spherical $Al_3(Sc,Zr)$ precipitates.

Microstructure Evolution During Hot Rolling

Prior to hot rolling, all samples were preheated at 500 °C/1.5 h and then hot-rolled at 500 °C. Typical microstructures after hot rolling are shown in Fig. 3. Because of the high reduction ratio (87%), the intermetallic particles were

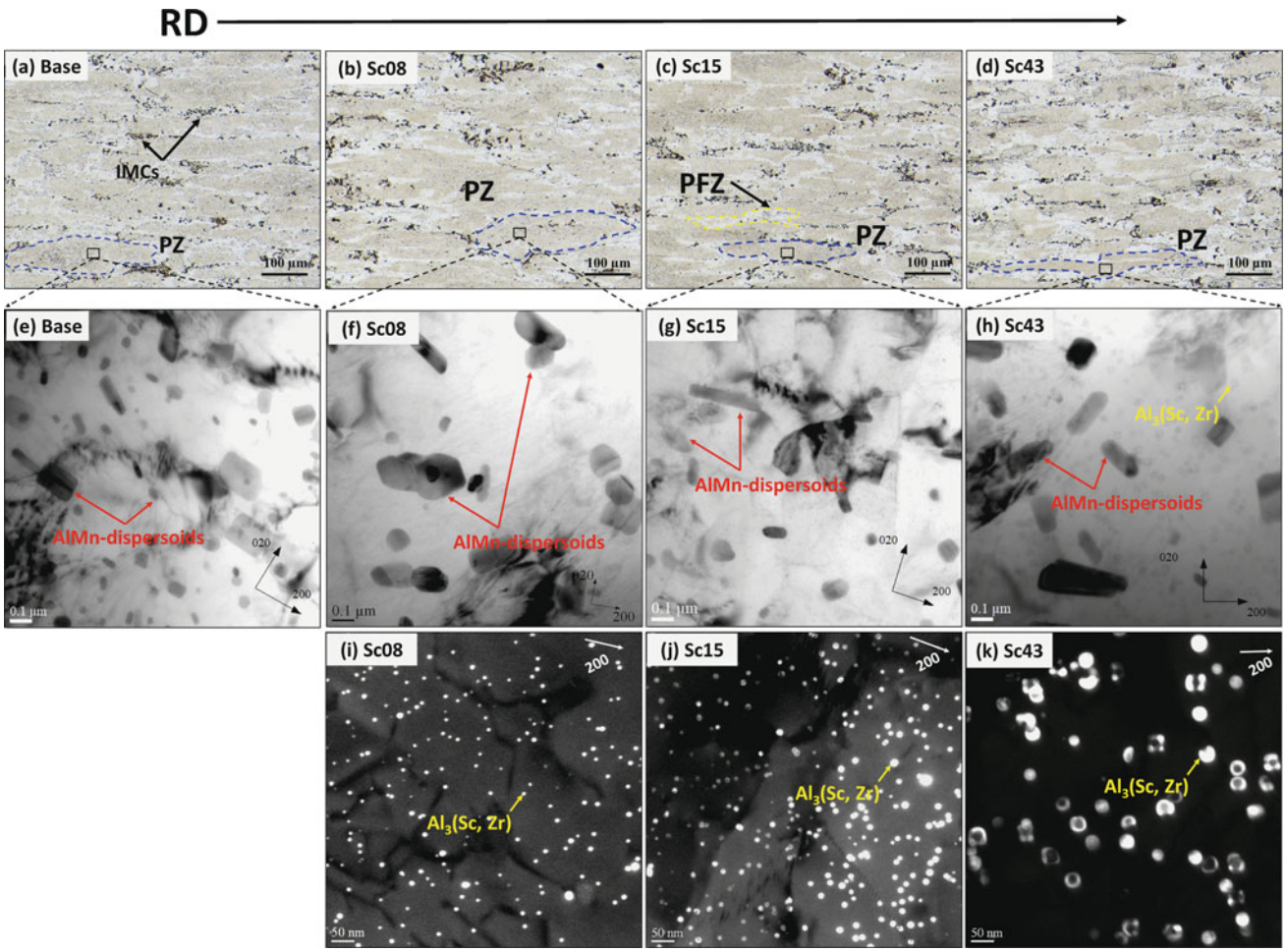

Fig. 3 Typical hot-rolled microstructures: (**a**, **b**, **c**, **d**) OM images and (**e**, **f**, **g**, **h**) bright-field TEM images showing the distribution of AlMn-dispersoids for Base, Sc08, Sc15, and Sc43; (**i**, **j**, **k**) dark-field TEM images showing the distribution of $Al_3(Sc,Zr)$ precipitates for Sc08, Sc15 and Sc43, respectively

fragmented, and the grains were elongated in the rolling direction, as shown in Fig. 3a–d. In addition, the line- and fan-shaped structures related to DCP in Sc43 completely disappeared. This could be attributed to the accelerated dissolution of the DCP rod-like precipitates due to the high rolling temperature (500 °C) and the accelerated diffusion rates during hot deformation [7, 22, 23].

Bright- and dark-field TEM images (Fig. 3e–h) and (Fig. 2i–k) revealed that both AlMn dispersoids and spherical $Al_3(Sc,Zr)$ precipitate coarsened during preheating and hot rolling as compared to the heat-treated alloys. This resulted in a size increase, and a significant decrease in number density (see Fig. 3 and Table 2). The quantitative results in Table 2 show that the number density of AlMn dispersoids decreased by 59%, 79%, and 76% during hot rolling for the Base, Sc15, and Sc43 alloys, respectively. Although the AlMn dispersoids coarsened, the number density in the base alloy was still higher than in Sc-containing alloys. On the other hand, the fine and spherical $Al_3(Sc,Zr)$ particles coarsened and exhibited a reduction in number density, particularly in the Sc43 alloy. For instance, the $Al_3(Sc,Zr)$ precipitate size increased during rolling by 104% and 107% in the Sc08 and Sc15 alloys, compared to 355% in the Sc43 alloy.

The reduced particle density and increased size of both AlMn dispersoids and $Al_3(Sc,Zr)$ precipitates after hot rolling are predominantly attributed to two factors. Firstly, the rolling temperature (500 °C) is higher than their formation temperature [7, 22]. Secondly, the high number density of dislocations generated during rolling accelerates the diffusion of alloying elements in the matrix, resulting in the growth and coarsening of both types of particles [23]. The most significant coarsening of spherical $Al_3(Sc,Zr)$ precipitates occurred in the Sc43 alloy (Fig. 3h), and the dissolved DCP $Al_3(Sc,Zr)$ further accelerates the coarsening of the spherical $Al_3(Sc,Zr)$ through the diffusion/growth mechanism, indicating their negative effect on the characteristics of the spherical $Al_3(Sc,Zr)$ precipitates [16].

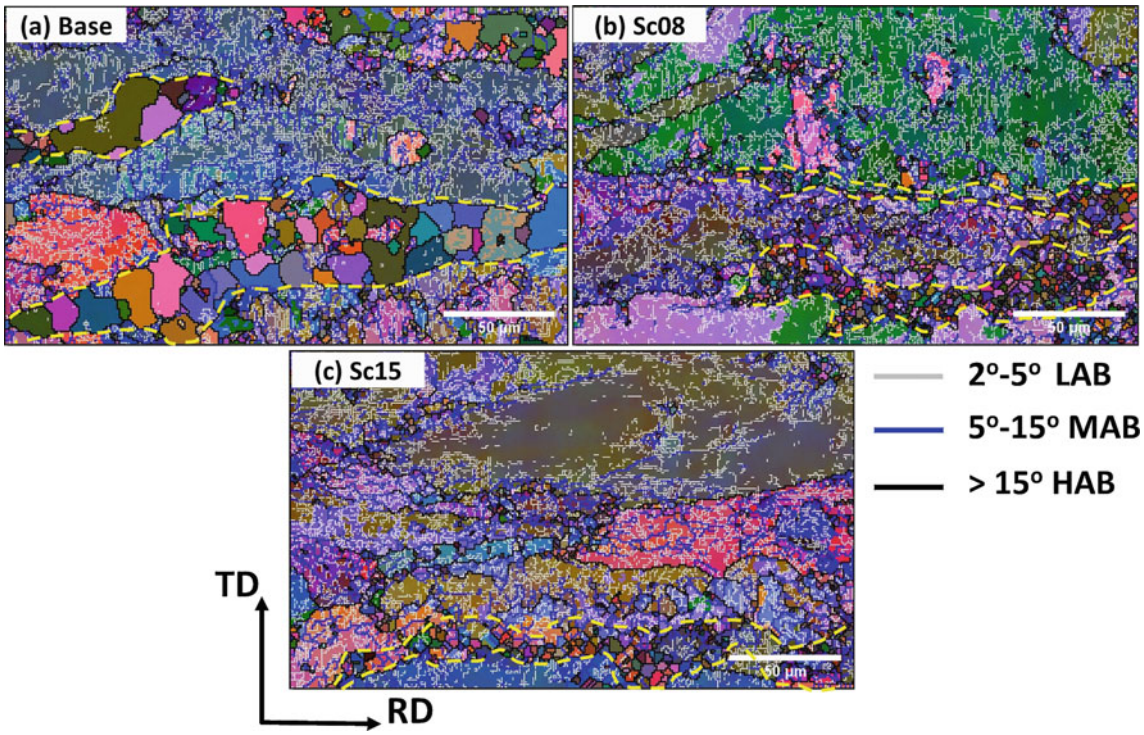

Fig. 4 All Euler orientation maps showing the grain structure after hot rolling and annealing

Figure 4 illustrates the grain structure of the base Sc08 and Sc15 alloys via Euler orientation maps after hot rolling and annealing. It can be seen that all samples exhibited a mixture of deformed grains in the rolling direction and recrystallized grains along the grain boundaries. In the base alloy, the recrystallized grains were coarser with an average size of 25 µm (marked by yellow dashed lines in Fig. 4a) and were randomly grown in the deformed grains. However, in the Sc-containing alloys, a chain of fine equiaxed and recrystallized grains (marked by yellow lines in Fig. 4b, c) was distributed along the grain boundaries with an average size of 3–8 µm. The lower fraction and the smaller size of recrystallized grains in the Sc-containing alloys can be explained by the effective pinning effect of Al_3(Sc,Zr) precipitates [3, 24, 25]. The predominant fibrous deformed grains along with the fine recrystallized grains in the Sc-containing alloys could provide additional strengthening at room temperature by inhibiting dislocation movement and grain rotation [26].

Mechanical Properties of Hot-Rolled Sheets

Figure 5 shows the microhardness of the experimental alloys after heat treatment and rolling. In general, the microhardness of the Sc-containing alloys was substantially higher than the base alloy, indicating the significant strengthening

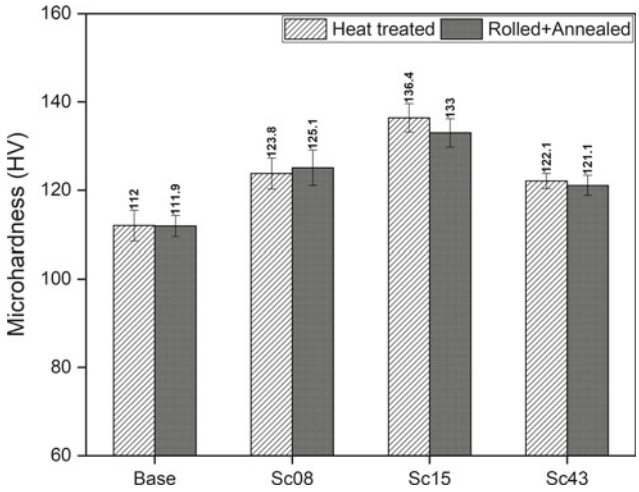

Fig. 5 Microhardness after heat treatment and hot rolling/annealing

effect of the nano-sized, spherical Al_3(Sc,Zr) precipitates. It can be seen that the microhardness value first increased with increasing Sc content, from the base alloy via Sc08 up to the Sc15 alloy, and then decreased significantly to the Sc43 alloy. The microhardness evolution after rolling and annealing showed a similar trend to the as heat-treated condition, corresponding to the substantial strengthening effect of the fine and spherical Al_3(Sc,Zr) precipitates (Fig. 3).

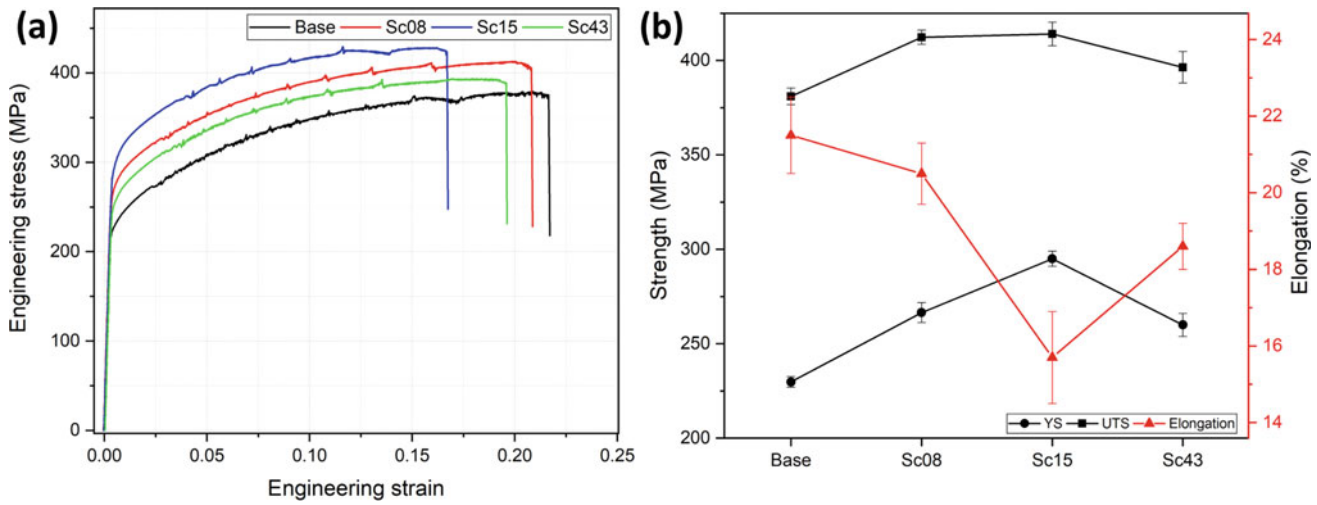

Fig. 6 **a** Typical engineering stress–strain curves of the rolled/annealed samples, and **b** the mean tensile properties versus Sc content

Figure 6 shows the ambient-temperature tensile properties of all four hot-rolled samples. Figure 6a demonstrates the typical engineering stress–strain curves. As shown in Fig. 6a, the stress level significantly increased with the addition of Sc and Zr, confirming the contribution of Sc towards improving the tensile properties. Figure 6b presents the tensile property data (YS, UTS and elongation). Similar to the microhardness trend, the YS and UTS initially increased with the Sc addition. The Sc15 alloy achieved the highest YS and UTS at 295 and 411 MPa, representing an improvement of 28% in YS and 8% in UTS relative to the base alloy. However, further increasing the Sc content to 0.43 wt.% significantly decreased the strength. For example, the Sc43 alloy gave a YS of 260 MPa, corresponding to an improvement of 13% compared to the base alloy, which was slightly lower than that of the Sc08 alloy.

As shown in Figs. 5 and 6, both the hardness and strength initially increased with increasing Sc addition up to 0.16% Sc, and then gradually degraded with further addition of Sc to 0.43%. These changes in mechanical properties are mainly attributed to the evolution of microstructures, especially the evolution of both AlMn dispersoids and spherical Al_3(Sc,Zr) precipitates. As illustrated in Fig. 2 and Table 2, with the addition of Sc and Zr, although the size of AlMn dispersoids increased and the number density decreased, the precipitation of a large number of fine and spherical Al_3(Sc, Zr) more than compensated for the loss of AlMn dispersoids, leading to the higher hardness in Sc-containing alloys (Fig. 5). During hot-rolling, although both AlMn dispersoids and spherical Al_3(Sc,Zr) coarsened (Fig. 3), the spherical Al_3(Sc,Zr) still effectively improved the mechanical properties due to their fine size and high number density. Meanwhile, the number density of fine and spherical Al_3(Sc, Zr) increased with the increasing Sc up to ~0.16%, which gave the highest mechanical properties. However, a decrease of both hardness and mechanical properties was observed with further addition of Sc (0.43%). This was principally associated with the formation of coarse discontinuous Al_3(Sc,Zr) in the as-cast condition, consuming more Sc and Zr from the solid solution. This resulted in a low number density of coarser spherical Al_3(Sc,Zr) precipitates after heat treatment (Fig. 3 and Table 2), resulting in the decreased hardness of Sc043 after heat treatment in Fig. 4. During hot-rolling, the released Sc and Zr solutes from the dissolution of discontinuous Al_3(Sc,Zr) further accelerated the coarsening of spherical Al_3(Sc,Zr) precipitates (Fig. 3k), leading to lower mechanical properties compared to the Sc15 alloy. However, the mechanical properties of the Sc43 alloy were still higher than the Sc-free base alloy, further confirming the positive contribution of nano-sized, spherical Al_3(Sc,Zr) precipitates on mechanical properties. However, due to the high cost of Sc, the addition of Sc should be well controlled to achieve the optimal mechanical properties for industrial applications, which is ~0.16 wt.% Sc based on the strength evolution in the context of this work.

Conclusions

(1) During multistep heat treatment, two strengthening phases (AlMn dispersoids and Al_3(Sc,Zr) precipitates) precipitated in the Sc/Zr-containing Al-Mg-Mn based alloys. However, the addition of Sc and Zr caused a reduction in number density of AlMn dispersoids. At high Sc levels (0.43 wt.%), the presence of coarse rod-like discontinuous Al_3(Sc,Zr) reduced the number density of fine and spherical Al_3(Sc,Zr) precipitates.

(2) During hot-rolling, both AlMn dispersoids and spherical Al_3(Sc,Zr) exhibited coarsening. More significant coarsening of spherical Al_3(Sc,Zr) particles occurred with the 0.43% Sc addition due to the dissolution of discontinuous Al_3(Sc,Zr).
(3) Hardness and strength increased with Sc additions up to 0.16 wt.%, followed by a decrease with further addition of Sc to 0.43 wt.%.
(4) In the hot-rolled and annealed condition, the highest strength was achieved with 0.16 wt.% Sc. The YS and UTS values of 295 and 411 MPa, respectively, represented improvements of 28% in YS and 8% in UTS compared to the base alloy free of Sc.

Acknowledgements The authors acknowledge the financial support from the Natural Sciences and Engineering Research Council of Canada (NSERC) and Rio Tinto Aluminum under the Grant No. CRDPJ 514651-17, through the Research Chair in Metallurgy of Aluminum Transformation at the University of Quebec at Chicoutimi.

References

1. J.R. Davis, (2001) Aluminum and aluminum alloys, light metals and alloys p 351–416. https://doi.org/10.1361/autb2001p351
2. J.A.V.D. Hoeven, L. Zhuang, (2002) A New 5xxx Series Alloy Developed for Automotive Applications, SAE TECHNICAL PAPER SERIES (724): 1-8. https://doi.org/10.4271/2002-01-2128
3. J. Jiang, F. Jiang, M. Zhang, Z. Tang, M. Tong, (2020) Recrystallization behavior of Al-Mg-Mn-Sc-Zr alloy based on two different deformation ways, Materials Letters 265: 127455. https://doi.org/10.1016/j.matlet.2020.127455
4. Y. Peng, S. Li, Y. Deng, H. Zhou, G. Xu, Z. Yin, (2016) Synergetic effects of Sc and Zr microalloying and heat treatment on mechanical properties and exfoliation corrosion behavior of Al-Mg-Mn alloys, Materials Science and Engineering A 666: 61-71. https://doi.org/10.1016/j.msea.2016.04.029
5. C.B. Fuller, J.L. Murray, D.N. Seidman, (2005) Temporal evolution of the nanostructure of Al(Sc ,Zr) alloys:Part I - Chemical compositions of Al3(Sc1-xZrx) precipitates, Acta Materialia 53(20): 5401-5413. https://doi.org/10.1016/j.actamat.2005.08.016
6. Y. Li, A. Muggerud, A. Olsen, T. Furu, (2012) Precipitation of partially coherent α-Al (Mn, Fe) Si dispersoids and their strengthening effect in AA 3003 alloy, Acta Materialia 60(3): 1004-1014. https://doi.org/10.1016/j.actamat.2011.11.003
7. K. Liu, X.G. Chen, (2015) Development of Al-Mn-Mg 3004 alloy for applications at elevated temperature via dispersoid strengthening, Materials and Design 84: 340-350. https://doi.org/10.1016/j.matdes.2015.06.140
8. A.Y. Algendy, K. Liu, X.G. Chen, (2021) Evolution of dispersoids during multistep heat treatments and their effect on rolling performance in an Al-5 % Mg-0 . 8 % Mn alloy, Materials Characterization 181:111487. https://doi.org/10.1016/j.matchar.2021.111487
9. Z. Li, Z. Zhang, X.G. Chen, (2018) Improvement in the mechanical properties and creep resistance of Al-Mn-Mg 3004 alloy with Sc and Zr addition, Materials Science and Engineering A 729: 196-207. https://doi.org/10.1016/j.msea.2018.05.055
10. A.Y. Algendy, K. Liu, P. Rometsch, N. Parson, X.G. Chen, (2022) Effects of AlMn dispersoids and Al3(Sc,Zr) precipitates on the microstructure and ambient/elevated-temperature mechanical properties of hot-rolled AA5083 alloys, Materials Science and Engineering: A 855: 143950. https://doi.org/10.1016/j.msea.2022.143950
11. A.K. Lohar, B. Mondal, D. Rafaja, V. Klemm, S.C. Panigrahi, (2009) Microstructural investigations on as-cast and annealed Al-Sc and Al-Sc-Zr alloys, Materials Characterization 60(11): 1387-1394. https://doi.org/10.1016/j.matchar.2009.06.012
12. J. Røyset, N. Ryum, (2005) Scandium in aluminium alloys, International Materials Reviews 50(1): 19-44. https://doi.org/10.1179/174328005X14311
13. D.N. Seidman, E.A. Marquis, D.C. Dunand, (2002) Precipitation strengthening at ambient and elevated temperatures of heat-treatable Al (Sc) alloys, Acta Materialia 50(16): 4021-4035. https://doi.org/10.1016/S1359-6454(02)00201-X
14. Q. Dong, A. Howells, D.J. Lloyd, M. Gallerneault, V. Fallah, (2020) Effect of solidification cooling rate on kinetics of continuous/discontinuous Al3(Sc,Zr) precipitation and the subsequent age-hardening response in cold-rolled AlMgSc(Zr) sheets, Materials Science and Engineering A 772: 138693. https://doi.org/10.1016/j.msea.2019.138693
15. Y. Sun, Q. Pan, Y. Luo, S. Liu, W. Wang, J. Ye, Y. Shi, Z. Huang, S. Xiang, Y. Liu, (2021) The effects of scandium heterogeneous distribution on the precipitation behavior of Al3(Sc, Zr) in aluminum alloys, Materials Characterization 174: 110971. https://doi.org/10.1016/j.matchar.2021.110971
16. A.K. Lohar, B.N. Mondal, S.C. Panigrahi, (2010) Influence of cooling rate on the microstructure and ageing behavior of as-cast Al–Sc–Zr alloy, Journal of Materials Processing Tech. 210(15): 2135-2141. https://doi.org/10.1016/j.jmatprotec.2010.07.035
17. K. Liu, E. Elgallad, C. Li, X.G. Chen, (2021) Effects of Zr and Sc additions on precipitation of α-Al(FeMn)Si dispersoids under various heat treatments in Al-Mg-Si AA6082 alloys, International Journal of Materials Research 112(9): 706-716. https://doi.org/10.1515/ijmr-2021-8283
18. L.L. Rokhlin, N.R. Bochvar, I.E. Tarytina, N.P. Leonova, (2010) Phase composition and recrystallization of Al-based Al-Sc-Mn-Zr alloys, Russian Metallurgy (Metally) 2010(3): 241-247. https://doi.org/10.1134/S0036029510030158
19. A.Y. Algendy, K. Liu, P. Rometsch, N. Parson, X.G. Chen, (2022) Evolution of discontinuous/continuous Al3(Sc, Zr) precipitation in Al-Mg-Mn 5083 alloy during thermomechanical process and its impact on tensile properties, Materials Characterization 192: 112241. https://doi.org/10.1016/j.matchar.2022.112241
20. Z. Li, Z. Zhang, X.G. Chen, (2018) Effect of Metastable Mg2Si and Dislocations on α-Al(MnFe)Si Dispersoid Formation in Al-Mn-Mg 3xxx Alloys, Metallurgical and Materials Transactions A: Physical Metallurgy and Materials Science 49(11): 5799-5814. https://doi.org/10.1007/s11661-018-4852-4
21. M.J. Starink, N. Gao, N. Kamp, S.C. Wang, P.D. Pitcher, I. Sinclair, (2006) Relations between microstructure, precipitation, age-formability and damage tolerance of Al-Cu-Mg-Li (Mn, Zr, Sc) alloys for age forming, Materials Science and Engineering A 418(1-2): 241-249. https://doi.org/10.1016/j.msea.2005.11.023
22. P. Xu, F. Jiang, M. Tong, Z. Tang, J. Jiang, N. Yan, Y. Peng, (2019) Precipitation characteristics and morphological transitions of Al3Sc precipitates, Journal of Alloys and Compounds 790: 509-516. https://doi.org/10.1016/j.jallcom.2019.03.256
23. M. Cabibbo, E. Evangelista, M. Vedani, (2005) Influence of severe plastic deformations on secondary phase precipitation in a 6082

Al-Mg-Si alloy, Metallurgical and Materials Transactions A 36(5): 1353-1364. https://doi.org/10.1007/s11661-005-0226-9

24. M. Li, Q. Pan, Y. Shi, X. Sun, H. Xiang, (2017) High strain rate superplasticity in an Al–Mg–Sc–Zr alloy processed via simple rolling, Materials Science and Engineering A 687 298-305. https://doi.org/10.1016/j.msea.2017.01.091
25. J. Jiang, F. Jiang, M. Zhang, Z. Tang, M. Tong, (2020) Al3(Sc, Zr) precipitation in deformed Al-Mg-Mn-Sc-Zr alloy: effect of annealing temperature and dislocation density, Journal of Alloys and Compounds 831: 154856. https://doi.org/10.1016/j.jallcom.2020.154856
26. A.H. Chokshi, (2020) Grain boundary processes in strengthening, weakening, and superplasticity, Advanced Engineering Materials 22(1): 1900748. https://doi.org/10.1002/adem.201900748